# Electronic Supplementary Information

## Controllable morphology transition from vesicular to worm-like to vesicular multilamellar mesoporous silica induced by *β*-cyclodextrin

Mengmeng Jiang, Shichao Li, Xue Shi, Tingting Gao, Zuohua Liu, Guowei Zhou*

*Key Laboratory of Fine Chemicals in Universities of Shandong, School of Chemistry and Pharmaceutical Engineering, Qilu University of Technology, Jinan, P. R. China.*

*Conresponding author: Tel: +86 531 89631696; Fax: +86 531 89631696

E-mail: gwzhou@qlu.edu.cn; guoweizhou@hotmail.com (G. W. Zhou)

## 1 Experimental

### 1.1 Chemicals

*β*-CD was purchased from the Sinopharm Chemical Reagent Co., with a water content of 14%. DDAB was purchased from Sigma–Aldrich. CTAB and TEOS were obtained from Shanghai Chemical Reagent, Inc. of the Chinese Medicine Group. Ammonia concentration of 25% was purchased from Tianjin Kemiou Chemical Reagent Co.. MH (content, >97%) was purchased from Aladdin. All chemicals were of analytical grade and used as received without any further purification. Millipore water 18.2 MΩ. cm (purified using an Milli-Q® Reference system) was used throughout all of the experiments.

### 1.2 Synthesis of MLS-n with a *β*-CD/CTAB/DDAB system

During synthesis, CTAB and DDAB were used as the structure-directing agents. *β*-CD plays a role in controlling aggregate transitions; thus, it was used as an inducing agent. First, 0.142 g of CTAB and 0.112 g of DDAB were dissolved in 35.00 mL of water to form a homogeneous solution. The resulting solution was stirred at 30 °C until the solution became clear. The desired amount of *β*-CD (0.05, 0.1, 0.15, 0.2, and 0.25 g in 5 different synthesis) was added into the solution for the preparation of a set of samples. The mixture was stirred until *β*-CD was completely dissolved. The resulting solution was added with 0.69 mL of ammonia before the aqueous solution was stirred for another 2 h. Second, 2.0 g TEOS was added dropwise under vigorous stirring. The reaction solution was constantly stirred at 30 °C for 24 h, transferred to a Teflon autoclave, and hydrothermally treated at 100 °C for another 24 h. Finally, the white solid products were collected by filtration, washed with water, and dried in air at room temperature. The as-synthesized samples were calcined at 550 °C for 6 h in

air to remove the organic templates.

**1.3 MH adsorption and release**

Drug storage and in vitro release profiles were obtained according to previously reported methods.[1-3] MH was selected as the model drug. The drug loading process was conducted by immersing the MLS-n (0.1 g) in 20 mL MH aqueous solution at a specific concentration (10 mg $mL^{-1}$) and at room temperature. The mixture was continuously stirred for 2 days at 35 °C to induce drug diffusion. Finally, the mixture was centrifuged at 6000 rpm for 10 min to obtain MH-loaded samples, which were dried at room temperature. The loading amount of MH was monitored with a UV–vis spectrophotometer at 233 nm. After MH loading, the respective MLS samples were labeled as MLS-0.05-MH, MLS-0.1-MH, MLS-0.15-MH, MLS-0.2-MH, and MLS-0.25-MH. The measurements were performed thrice for each sample, and the results were averaged. The drug loading amount was then calculated as Equ. S1:

$$wt.\% = \frac{m_1 - \frac{20}{v}CV}{m_2 + \left(m_1 - \frac{20}{v}CV\right)} 100\% \qquad \text{S(1)}$$

where $m_1$ and $m_2$ correspond to the initial mass of MH and mesoporous materials added into aqueous solution, respectively. $C$ is the concentration of filtrates diluted in 20 mL volumetric flask, $v$ is sampled volume from filtrates, and $V$ is the volume of aqueous solution for drug loading.

For the release profiles, 100 mg of the loaded sample was placed in 50 mL PBS (pH = 6.8). The contents were stirred at 100 rpm and 37 °C. At predetermined frequencies, 3 mL of the mixture was collected and replaced with the same volume of fresh PBS. The extracted mixture was passed through a 4.5 μm membrane filter and monitored with a UV–vis spectrophotometer. The measurements were performed thrice for each sample, and the results were averaged. The actual concentration of

released MH according to the following Equ. S2:

$$C_{\text{t-cor}} = C_{\text{t}} + \frac{v}{V}\sum_{0}^{t-1} C_{\text{t}} \qquad \text{S(2)}$$

where $C_{\text{t-cor}}$ is the actual concentration of released MH at time t (mg $mL^{-1}$), $C_t$ is the apparent drug concentration at time t (mg $mL^{-1}$), $v$ is the removed volume of release fluid (mL), and $V$ is the total volume of release fluid (mL).

**1.4 MH release kinetics analysis**

Kinetics release data were analyzed using the first-order model. The first order kinetic release is concentration dependant and can be expressed as:

$$\log C_{\text{t}} = \log C_{\text{o}} - k_1 \cdot \text{t}/2.303 \qquad \text{S(3)}$$

where $C_t$ is the concentration of drug released in time t, $C_o$ is the initial concentration of drug present in the $mSiO_2$ nanoparticles, and $k_1$ is the first-order rate constant. The value of $k_1$ was calculated from the slope of the linear plot of log cumulative % drug remaining versus time (Figure S7).

**1.5 Materials characterizations**

High-resolution transmission electron microscopy (HRTEM) measurements were carried out on JEM-2100 at accelerating voltage of 200 kV. All samples were dispersed in ethanol ultrasonically and were dropped on copper grids, and dried in air. Field emission scanning electron microscopy (FESEM) micrographs of samples were obtained by a Hitachi S-4800 microscope operated at an acceleration voltage of 5.0 kV. Powder samples were dispersed in ethanol by sonication, then dropped onto the surface of silicon wafer and were sputter-coated for 2 cycles with gold to avoid charging under the electron beam prior to examination. The small-angle X-ray powder diffraction (SAXRD) patterns were recorded using a Bruker D8 advance diffractometer with Cu Kα radiation (35 kV, 30 mA, $\lambda$ = 0.15406 nm). The data were

collected from $2\theta$ = 0.5-5° with a resolution step size of 0.02° $s^{-1}$ and a scan step time of 5 s. $N_2$ adsorption-desorption experiments were measured on TriStar 3020 and QuadraSorb SI of Quantachrome Instruments. Samples were degassed for 8 h at 120 °C before measurements. Specific surface areas were calculated by Brunauer-Emmett-Teller (BET) method, the pore size distribution and volumes were calculated from the adsorption branch using Barett–Joyner–Halenda (BJH) methods. The $N_2$-adsorption experiments were replicated three times and the results were averaged. UV-vis spectra were recorded on a SHIMADZU UV-2600 spectrophotometer. Thermogravimetric analysis (TGA) was performed on a TGA 1500 DSP-SP instrument at a heating rate of 20 °C $min^{-1}$ from room temperature to 1000 °C under air atmosphere. Fourier transform infrared (FT-IR) spectra were recorded on an IRPrestige-21 spectrometer with a resolution of 4 $cm^{-1}$ and a scan number of 32 by using compressed KBr discs containing 1 wt% of the sample. For cross polarization magic angle spinning nuclear magnetic resonance spectroscopy (CP-MAS NMR) measurements, the samples were pressed into 4 mm zirconia rotors and spun at 14 kHz. The measurements were conducted on a Bruker AvanceIII 400 spectrometer (Bruker BioSpin, Rheinstetten, Germany) with a resonance frequency of 100.62 MHz for $^{13}C$. The signal-to-noise ratio was enhanced by applying cross polarization. The contact time was 2000 us, the relaxation delay was 1 s, a ramp-contact and spinal64 decoupling pulse program was used. The spectra were recorded as the sum of 2000 scans and calibrated using the methine carbon atoms of adamantane as an external standard ($\delta$ = 29.47 ppm).

## 2 Characterization data

### 2.1 TEM images

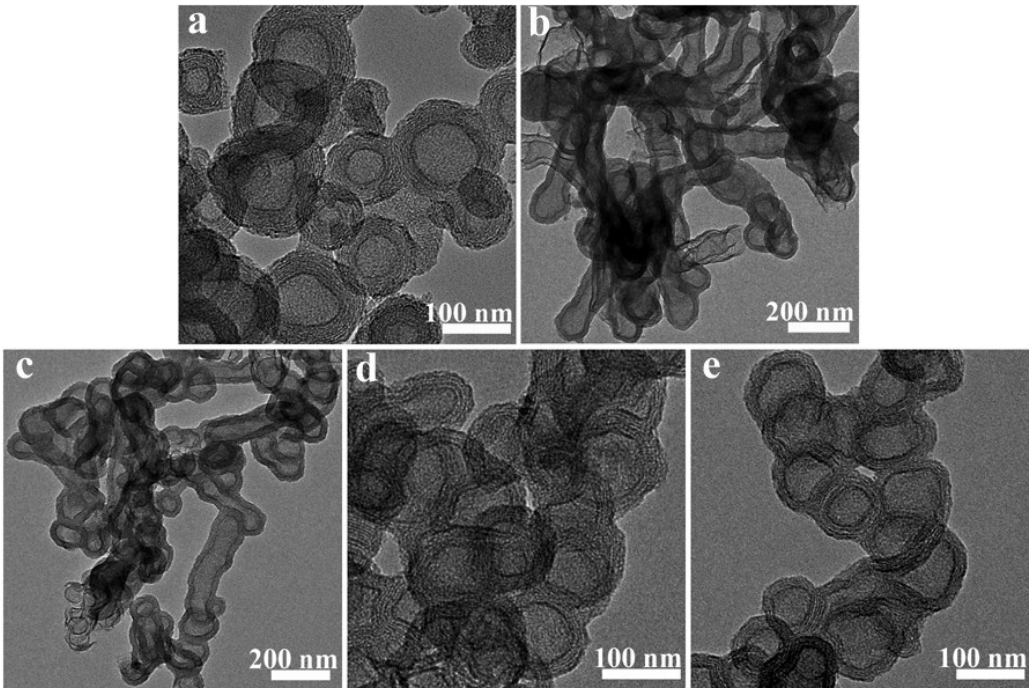


**Fig. S1** HRTEM images of (a) MLS-0.05, (b) MLS-0.1, (c) MLS-0.15, (d) MLS-0.2, and (e) MLS-0.25.

## 2.2 SEM images

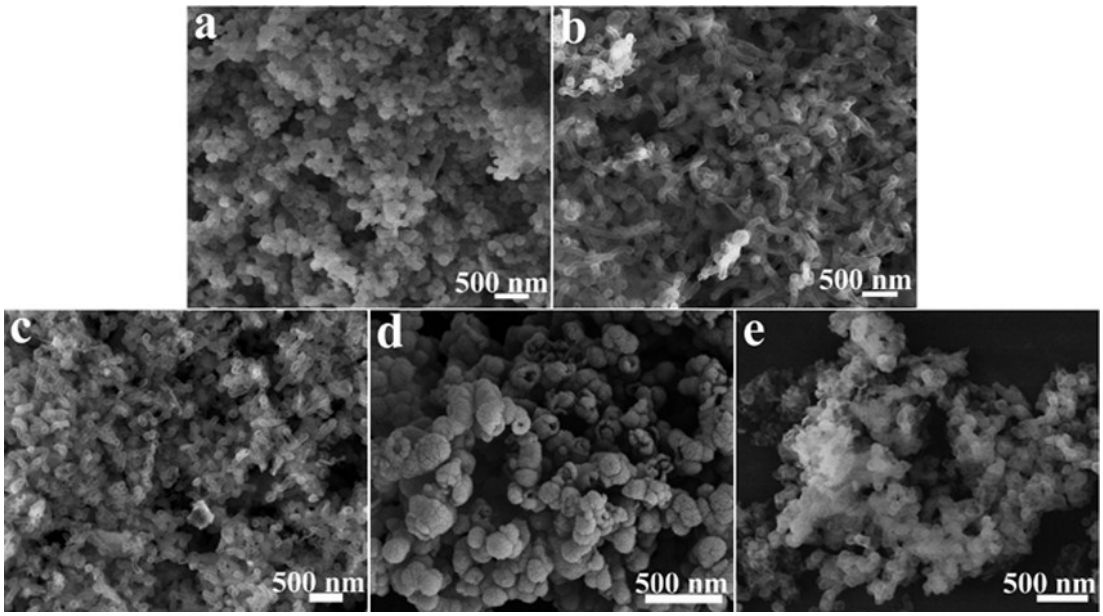


**Fig. S2** FESEM images of (a) MLS-0.05, (b) MLS-0.1, (c) MLS-0.15, (d) MLS-0.2, and (e) MLS-0.25.

## 2.3 XRD patterns

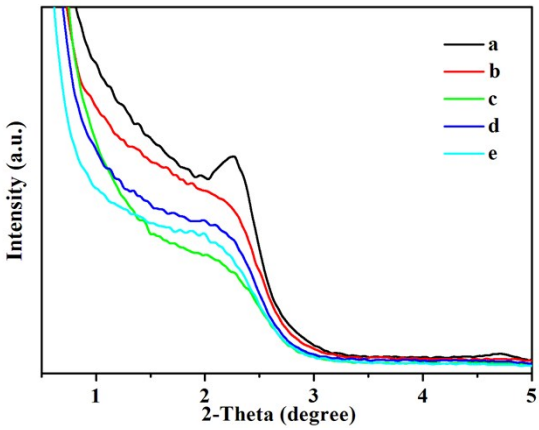


**Fig. S3** SAXRD patterns of MLS-0.05 (a), MLS-0.1 (b), MLS-0.15 (c), MLS-0.2 (d), and MLS-0.25 (e).

### 2.4 $N_2$ adsorption-desorption isotherms

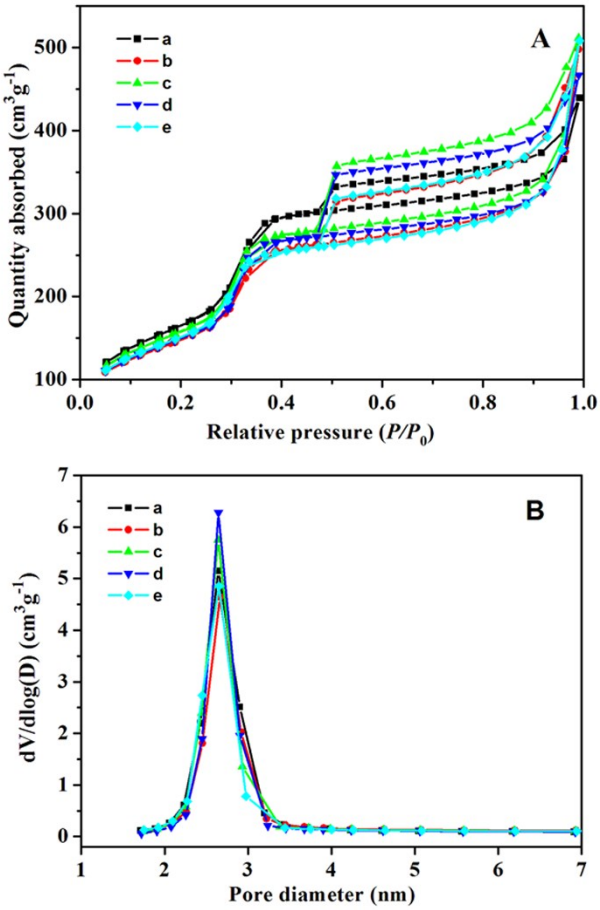


**Fig. S4** (A) Nitrogen adsorption–desorption isotherms and (B) corresponding BJH pore size distribution curves of (a) MLS-0.05, (b) MLS-0.1, (c) MLS-0.15, (d) MLS-0.2, and (e) MLS-0.25.

## 2.5 Structure parameters of MLS-n

**Table S1** Structure parameters of MLS-n before and after MH adsorption

| Sample | $S_{BET}$ ($m^2$ $g^{-1}$) | $V$ ($cm^3$ $g^{-1}$) | $D$ (nm) |
|---|---|---|---|
| MLS-0.05 | 602 | 0.70 | 2.70 |
| MLS-0.1 | 536 | 0.79 | 2.76 |
| MLS-0.15 | 573 | 0.81 | 2.68 |
| MLS-0.2 | 543 | 0.74 | 2.70 |
| MLS-0.25 | 551 | 0.80 | 2.71 |
| MLS-0.05-MH | 534 | 0.65 | 2.60 |
| MLS-0.1-MH | 465 | 0.72 | 2.49 |
| MLS-0.15-MH | 420 | 0.72 | 2.50 |
| MLS-0.2-MH | 479 | 0.59 | 2.25 |
| MLS-0.25-MH | 412 | 0.62 | 2.48 |

$D$, $S_{BET}$, and $V$ stand for interlamellar voids, surface area, and pore volume, respectively.

## 2.6 $N_2$ adsorption-desorption isotherms after loading MH

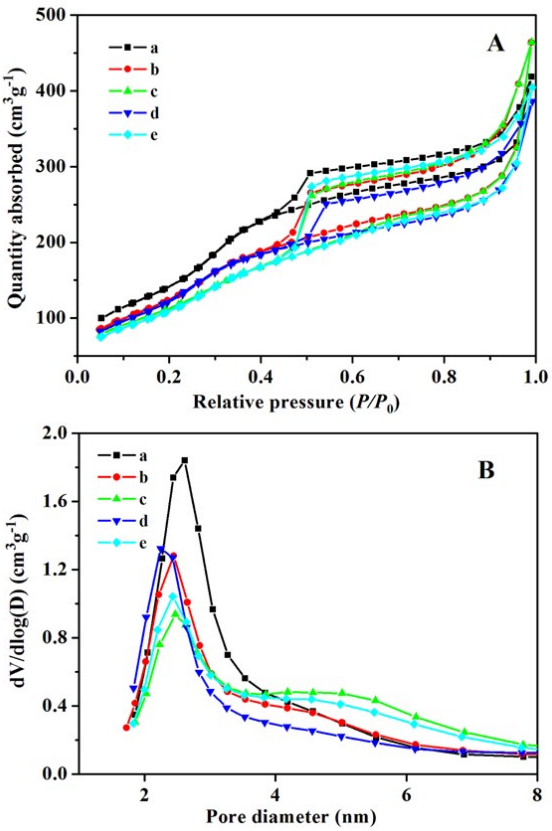


**Fig. S5** (A) $N_2$ adsorption-desorption isotherms and (B) corresponding BJH pore size distribution curves of (a) MLS-0.05-MH, (b) MLS-0.1-MH, (c) MLS-0.15-MH, (d) MLS-0.2-MH, and (e) MLS-0.25-MH.

## 2.7 MH release profiles

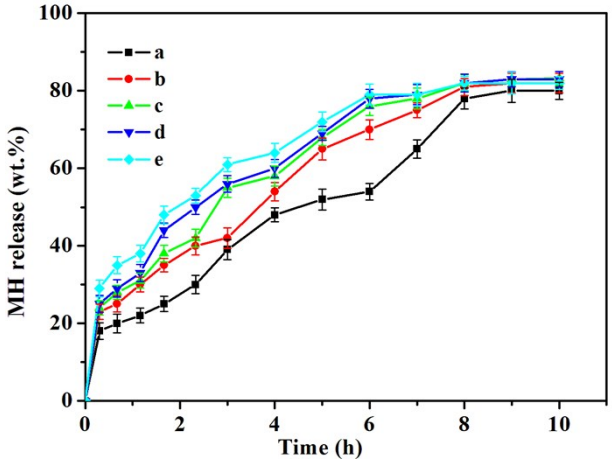


**Fig. S6** The mean cumulative release rates of MH in PBS of pH = 6.8 (a) MLS-0.05-MH, (b) MLS-0.1-MH, (c) MLS-0.15-MH, (d) MLS-0.2-MH and (e) MLS-0.25-MH.

## 2.8 Drug release kinetics

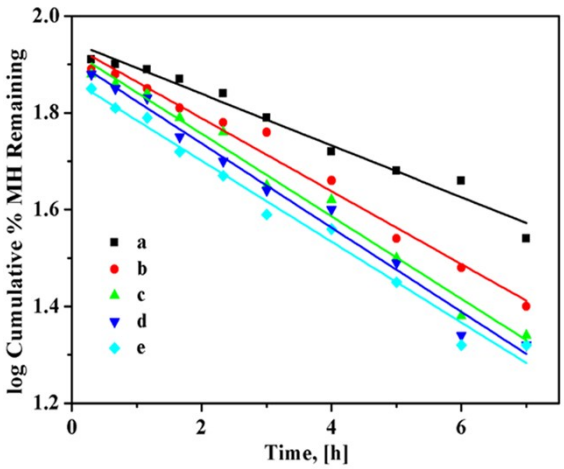


**Fig. S7** Release first-order kinetic model of MH from (a) MLS-0.05-MH, (b) MLS-0.1-MH, (c) MLS-0.15-MH, (d) MLS-0.2-MH and (e) MLS-0.25-MH.

**Table S2** Correlation coefficients and kinetic constants for release of MH from MLS-n.

| Sample | First-order model | |
|---|---|---|
| | $k_1$ | $R^2$ |
| MLS-0.05-MH | 0.053 | 0.972 |
| MLS-0.1-MH | 0.075 | 0.982 |
| MLS-0.15-MH | 0.085 | 0.985 |
| MLS-0.2-MH | 0.087 | 0.984 |
| MLS-0.25-MH | 0.084 | 0.982 |

$k_1$ and $R^2$ stand for kinetic constant and correlation coefficients, respectively.

**2.9 TG analysis of MLS-n**

The TG analysis of MLS-n before (A) and after (B) calcination was performed after vacuum-drying the samples at 40 °C for 48 h (**Fig. S8**). **Fig. S8**(A) shows that all samples had an initial weight loss at approximately100 °C because of the physically adsorbed water. The significant weight loss between 120 °C and 500 °C, with a weight loss of approximately 24 wt%, was mainly caused by the decomposition of

surfactant CTAB and DDAB. Calcination (B) of MLS-n also resulted in a weight loss at approximately100 °C because of the adsorbed water. However, no distinct surfactant weight loss after 100 °C because of the prior calcination at 550 °C.

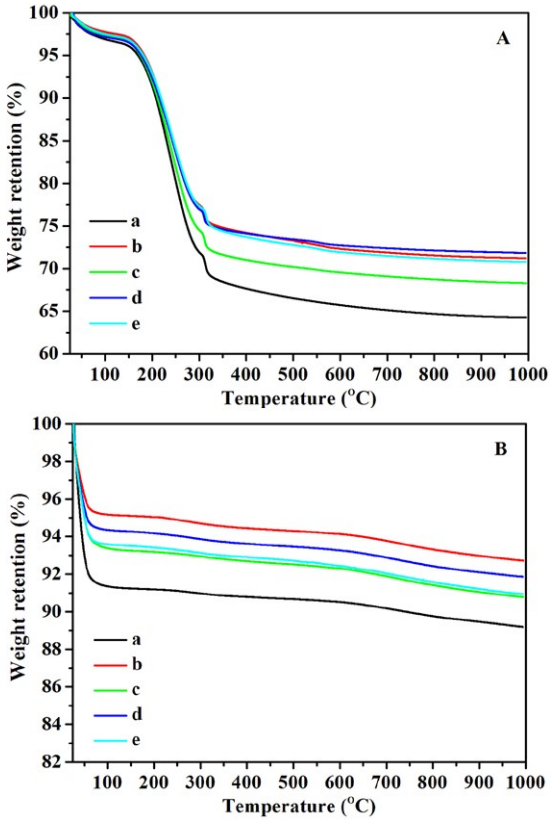


**Fig. S8** TG curves of MLS-n before (A) and after calcination (B) of (a) MLS-0.05, (b) MLS-0.1, (c) MLS-0.15, (d) MLS-0.2, and (e) MLS-0.25.

**2.10 FT-IR analysis of MLS-n**

The FT-IR spectra of MLS-n before and after calcination are shown in **Fig. S9**(A) and (B), respectively. The peak in Fig. S9(A) centered at 3425 $cm^{-1}$ was assigned to surface hydroxylation OH stretching mode of the framework Si-O-H. The presence of intense absorption band at approximately1095 $cm^{-1}$ was due to the asymmetric Si-O-Si stretching vibration modes, whereas the band at 804 $cm^{-1}$ was attributed to symmetric Si-O-Si stretching vibration. The absorption peaks at 469 and 968 $cm^{-1}$ belonged to Si-O-Si bending vibration and stretching vibration of Si-OH surface groups, respectively. These absorption bands indicate the formation of $SiO_2$

nanoparticles.[4] Two weak adsorption peaks were found at 2856 and 2927 $cm^{-1}$, which are the stretching vibration peaks of saturated hydrocarbons of $-CH_3$ and $-CH_2$ in CTAB and DDAB. However, no $-CH_2$ and $-CH_3$ group absorption peaks were observed in the FT-IR spectra of MLS-n after calcination (**Fig. S9**(B)). These results indicate that the surfactant CTAB and DDAB have been decomposed during the calcination process.

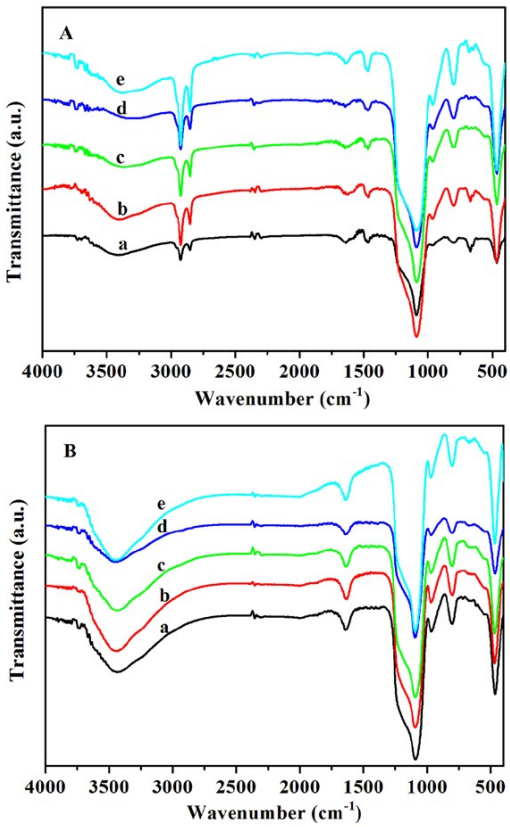


**Fig. S9** FT-IR spectra of MLS-n before (A) and after (B) calcination of (a) MLS-0.05, (b) MLS-0.1, (c) MLS-0.15, (d) MLS-0.2, and (e) MLS-0.25.

### 2.11 $^{13}C$ CP-MAS NMR analysis of MLS-n

**Fig. S10** shows the $^{13}C$ CP-MAS NMR spectra of MLS-n before calcination. Seven peaks at 22.77, 26.28, 30.42, 32.32, 53.86, 62.54, and 66.96 ppm denote the presence of seven different carbon chemical environments.[5] These peaks could be attributed to the surfactant CTAB and DDAB in MLS-n before calcination. However,

the four major signals of $\beta$-CD at approximately 60.15, 72.99, 80.62, and 103.49 ppm were not observed in **Fig. S10**, which indicates that $\beta$-CD did not exist in the channels in this series of MLS-n before calcination.[6] These findings are consistent with the TGA and FT-IR results.

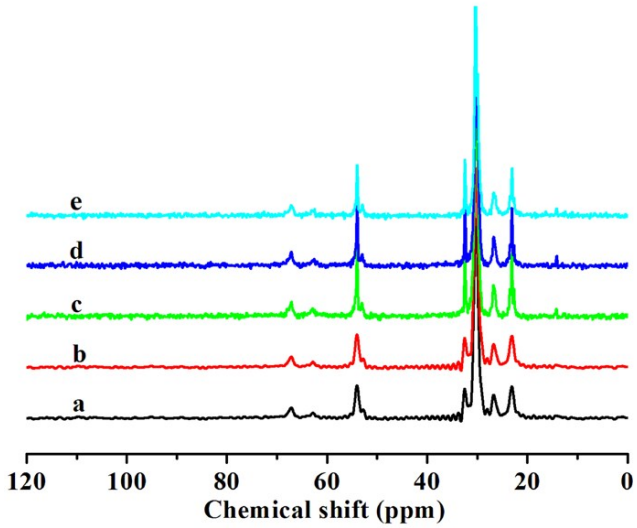


**Fig. S10** $^{13}$C CP-MAS NMR of MLS-n before calcination of (a) MLS-0.05, (b) MLS-0.1, (c) MLS-0.15, (d) MLS-0.2, and (e) MLS-0.25.

**References**

1 P. K. Choudhury and M. KAR, Journal of Microencapsulation, 2009, **26**, 46.

2 A. A. Hasan, H. Madkor and S. Wageh, Drug Deliv, 2013, **20**, 120.

3 C. L. N. Reddy, B. Y. Swamy, C. V. Prasad, K. M. Rao, M. N. Prabhakar, C. Aswini, M. C. S. Subha and K. C. Rao, International Journal of Polymeric Materials, 2012, **61**, 424.

4 M. M. Ayad, N. A. Salahuddin, N. L. Torad and A. A. El-Nasr, RSC Adv., 2016, **6**, 57929.

5 R. Simonutti, A. Comotti, S. Bracco and P. Sozzani, Chem. Mater., 2001, **13**, 771.

6 M. J. Ferreira, A. García, D. Leonardi, C. J. Salomon, M. C. Lamas and T. G. Nunes, Carbohydrate Polymers, 2015, **123**, 130.